A high potent synthetic nanobody with broad-spectrum activity neutralizes SARS-Cov-2 virus and Omicron variant through a unique binding mode

Dongping Zhao[1,2#], Liqin Liu[3,4#], Xinlin Liu[2,5#], Jinlei Zhang[3#], Yuqing Yin[1], Linli Luan[1], Dingwen Jiang[1], Xiong Yang[6], Lei Li[2,5], Hualong Xiong[3], Dongming Xing[2,5], Qingbing Zheng[3,4], Ningshao Xia[3,4], Yuyong Tao[7*], Shaowei Li[3,4*] and Haiming Huang[8,¶*]

1 Noventi Biopharmaceuticals Co., Ltd, Shanghai, 201203, China.

2 School of Basic Medicine and the Affiliated Hospital of Qingdao University, Qingdao University, Qingdao, 266071, China.

3 State Key Laboratory of Molecular Vaccinology and Molecular Diagnostics, School of Public Health, School of Life Sciences, Xiamen University, Xiamen, 361102, China.

4 National Institute of Diagnostics and Vaccine Development in Infectious Diseases, Xiamen University, Xiamen, 361102, China.

5 The Cancer Institute, Qingdao University, Qingdao, 266071, China.

6 Guangxi Asia United Antibody Medical Co., Ltd, Hezhou, Guangxi, 542899, China

7 Department of Clinical Laboratory, The First Affiliated Hospital of USTC, Ministry of Education Key Laboratory for Membraneless Organelles & Cellular Dynamics, Biomedical Sciences and Health Laboratory of Anhui Province, School of Life Sciences, Division of Life Sciences and Medicine, University of Science and Technology of China, 230027, Hefei, P.R. China.

8 Shanghai Asia United Antibody Medical Co., Ltd, Shanghai, 201203, China

[#] These authors contributed equally to this work.

* To whom correspondence should be addressed.

¶ Present address: Noventi Biopharmaceuticals Co., Ltd, Shanghai, 201203, China.

E-mail: Haiming Huang(haiming.huang@auambio.com) ,

Shaowei Li(shaowei@xmu.edu.cn.)

Yuyong Tao(taoyy@ustc.edu.cn)

Abstract

COVID-19 continues to be a severe public health thread worldwide. The major challenge to control this pandemic is the rapid mutation rate of the SARS-Cov-2 virus, leading to the escape of the protection of vaccines and most of the neutralizing antibodies to date. Thus, it is pivotal to develop neutralizing antibodies with broad-spectrum activity targeting multiple SARS-Cov-2 variants. Here, we first got a synthetic nanobody(named C5) which could interfere with ACE2 binding to SARS-Cov-2 spike protein and its RBD domain. The affinity matured format of C5 clone, named C5G2, has a single digit nanomolar affinity to RBD domain and inhibit its binding to ACE2 with an IC_{50} of 3.7 nM. Pseudovirus assay indicated that the monovalent C5G2 could protect the cells from the infection of SARS-Cov-2 wild type virus and most of the virus of concern, i.e. Alpha, Beta, Gamma and Omicron variants. Strikingly, C5G2 has the highest potency against omicron among all the variants with the IC50 of 4.9ng/ml(0.3n M). We further solved the Cryo-EM structure of C5G2 in complex with the Spike trimer. The structure data showed that C5G2 bind to RBD mainly through its CDR3 at a vast region that not overlapping with the ACE2 binding surface. Surprisingly, C5G2 also bind to a distinct epitope residing in the NTD domain of spike protein through the same CDR3 loop, which may further increase its potency against the virus infection. Thus, this bi-paratopic nanobody may be served as an effective drug for the prophylaxis and therapy of the Omicron infection.

Keywords: SARS-Cov-2, Neutralizing antibody, synthetic nanobody, broad-spectrum, Omicron, Cryo-EM, bi-paratope

Introduction

COVID-19 (coronavirus disease 2019) has been a pandemic worldwide since the end of 2019. As of Feb 25th 2022, it has caused more than 420 million infection cases and more than 6 million deaths(https://covid19.who.int/). It is SARS-CoV-2, which belongs to the beta coronavirus family, that cause the disease[1, 2]. SARS-CoV-2 virus enter human cells via its spike protein, which is capable of binding to the ACE2(angiotensin-converting enzyme 2) receptors on the surface of the host cells[3, 4]. The spike protein is composed of S1 subunit at its N-termini and S2 subunit at its C-termini[5]. The S1 contains a N-terminal domain(NTD) and a receptor binding domain(RBD) which engages the binding to the ACE2 receptors of the host cells[5-7]. Upon the binding, S2 subunit will mediate the membrane fusion between the viral and host cells to finish the viral entry[8, 9]. Based on this biological process, spike protein has been the target for neutralising antibody therapy and vaccine protection[10-14]. However, the rapid mutation rate of SARS-CoV-2 challenges the development of neutralising antibody and vaccine.

There are two groups of neutralising antibodies targeting spike protein of SARS-CoV-2, the majority of which are those binding to RBD, thus blocking virus interaction with ACE2[10, 11, 15, 16]. In addition, antibodies targeting NTD could also have neutralization efficacy[17, 18]. The mechanism of anti-RBD neutralising antibodies could also be classified into two groups[19]. The first group of antibodies bind to RBD and blocked its interaction with ACE2 directly, thus protecting the host cells from virus infection[10, 20-23]. On the contrary, the other group of antibodies interact with RBD at epitopes distinct from the binding interface between RBD and ACE2, resulting virus entry prevention as well, due to partially, if not all, the conformation changes of RBD[24] [25]. This type of neutralising antibodies is more likely to act as the wide spectrum antibodies as they bind to the conserved residues at RBD/NTD across the SARS-CoV-2 variants.

The neutralising antibodies were mainly derived from B cells of COVID-19 patients and immunized animals[26, 27] or phage displayed antibody libraries, either naturally origin or synthetic ones[10, 11, 20]. The synthetic antibody library technology harnesses the frameworks of natural antibodies, based on which only the CDRs(Complementarity-determining regions) were partially or completely randomized to form large content(diversity usually greater than 10^9 pfu) libraries[28-30]. Though independent of immune system, the notion of synthetic antibody as therapeutic has been proved feasible and practical as exemplified by MorphoSys antibody drug guselkumab. The guselkumab, targeting IL23, was developed from MorphoSys synthetic library HuCAL and approved to treat plaque psoriasis by FDA in 2017[31-34]. HuCAL library was constructed using human germlines as scaffolds[35]. Since then, many different antibody scaffolds have been employed to generate synthetic antibody libraries, including nanobodies. Nanobodies or single domain antibodies are the variable regions of the heavy-chain only antibodies that from Camelid immune system[36, 37]. One of the benefits of using nanobodies to construct synthetic antibody libraries is that a nanobody has only three CDRs(*versus* six CDRs in a conventional antibody) , which makes the mutation process easier than those of using conventional IgG(Fab or scFv fragment) as scaffolds[38]. There are many nanobodies, either natural[11, 39] or synthetic ones[10, 40], have been reported that have neutralising activity against SARS-CoV-2 virus. Unfortunately, there are few nanobodies reported to date that have broad spectrum neutralising activity against multiple SARS-CoV-2 variants, especially the newly emerged Omicron.

We firstly described in this study the construction of a synthetic nanobody library based on a camel nanobody by a unique randomization strategy. We selected this library against SARS-CoV-2 spike protein, S1 subunit and RBD domain, respectively by phage display and obtained seven nanobodies in total. One of the RBD binding nanoboides, named C5, is capable of competing with ACE2 to bind to RBD. Protein engineering technology was applied to improve the binding affinity of C5 to RBD and its solubility and yield. The engineered variant, i.e. C5G2, has been proved its potency to protect living cells from infection by SARS-CoV-2 pseudovirus. In addition, C5G2 could inhibit multiple variants, including the Omicron, infecting living cells with high potency in pseudovirus assay. We further solved the cryo-EM structure of C5G2 in complex

with the spike protein trimer, uncovering the structural basis of the broad-spectrum neutralising activity. Intriguingly, the structure also shows that C5G2 is a bi-paratopic nanobody, which interacts with not only RBD but also NTD of the spike protein trimer simultaneously through a single CDR3 loop.

Results

The design, construction and quality control of a synthetic nanobody library

In order to obtain antibodies for diverse antigens by phage display, we firstly sought to construct a synthetic nanobody library. To this end, a natural nanobody (PDB no. 1ZVH) [41], which recognizes lysozyme, was selected as the template for the library construction (Figure 1A). In our library design, residues from 27 to 33 of complementarity-determining region 1 (CDR1), 51 to 58 of CDR2 and 99 to 112 of CDR3 were randomized simultaneously (Figure 1A). The length of each CDR in the library were kept the same as the template. At each position of the CDRs, an amino acid mix were incorporated by Kunkel method[42, 43]. The amino acid mix(X) is composed of 19 natural amino acids, excluding cysteine (Figure 1A) to prevent the forming of unexpected disulfide bond though extra interloop disulfide bond is very common in the natural occurring nanobodies, especially camel derived ones [36] . The detail of the construction of the library was described in the Material&Methods section. The resultant diversity of the library was ~3×10^9 colony-forming units (cfu). The DNA deep sequencing result indicated that the mutated molecules have expected amino acid ration as designed at each CDR (Figure 1B). This library was then named AUAM synthetic nanobody library (ASyNAL).

To test the application of this library, we then panned the library against seven diverse antigens by phage display. Other than lysozyme, those antigens were cytoplasmic proteins i.e. SH2 domain of Tyrosine-protein kinase Fyn (Fyn_SH2) and Glutathione S-transferase (GST), extracellular domain of cell membrane proteins i.e. Human Epidermal Growth Factor Receptor 2 (Her2), Siglec15 and virus proteins i.e. human SARS-CoV-2 spike protein and Porcine Circovirus (PCV) 2d protein. As shown in Table 1, we were able to obtain at least one nanobody for each of those seven antigens verified by phage ELISA, indicating the versatile applications of ASyNAL in generation of nanobodies for diverse antigens.

Characterization of potential neutralizing nanobody against SARS-CoV-2 spike protein

In an attempt to obtain neutralizing nanobody against SARS-CoV-2, we panned the ASyNAL library against three antigens including the spike protein, S1 domain and RBD, respectively. As a result, we successfully obtained six spike-specific nanobodies (named C5, D3, D8, D9, F12 and G2), one S1-specific nanobody (A11) and one RBD-specific nanobody (B7) (Figure 2A-C, Table S1, Figure S1). DNA sequencing showed that D3 clone (from spike panning) and A11 (from S1 panning) are sequentially identical. Thus, we totally got seven unique nanobodies for spike protein. To map the binding epitopes of those nanobodies, we then applied cross-reactive phage ELISA assay to check the bindings of those seven nanobodies to spike protein and its fragments, respectively. All seven nanobodies bound the spike protein as expected (Figure 2A). Furthermore, they all bound to S1 as well (Figure 2B), but only nanobodies B7 and C5 could bind to the RBD (Figure 2C), implying those five clones are likely NTD binders (Figure S1A). In a competitive ELISA, NTD binding nanobodies D8, D9, F12 and G2, but not RBD binder B7, inhibit D3 phage binding to spike protein (Figure S1B), showing they may share the same (or overlapping) epitope as D3 clone in the NTD domain (Figure S1A&Table S1).

The binding affinities of those nanobodies to their screening antigens (spike, S1 or RBD) were measured by Bio-Layer Interferometry (BLI). As shown in Table 2, the binding affinities (KD) are ranging from 10^{-10} M to 10^{-7} M, which are similar to those selected from synthetic nanobody libraries[10] as well as natural nanobody libraries[11]. Furthermore, we investigated the size exclusion chromatography (SEC) profiles of the nanobodies and the result indicated that, other than C5 which has aggregation (data not shown), five nanobodies (B7, D8, D9, F12, G2) showed one single peak and nanobody A11 and D3 showed minimal (~5%) aggregation (Figure S2).

As the spike protein of SARS-CoV-2 binds to human Angiotensin-converting enzyme 2 (ACE2) through its RBD domain to initiate the entry of the virus into human cells, we wonder if the RBD-specific nanobodies B7 and C5 identified in this study could interfere with the binding of ACE2 to the RBD. Unfortunately, the yield of C5 protein was very poor when expressed in the bacterial host BL21. So we were unable to use C5 protein as competitor to interfere with the binding of spike protein to the ACE2 by competitive ELISA. On the contrary, we tried to use ACE2 to interfere with the binding of C5/B7 nanobodies displayed on phage to S protein and RBD(i.e. phage competitive ELISA). As shown in Figure 2D, the binding of C5, but not B7, to RBD

could be inhibited when using ACE2 protein as the competitor. Furthermore, the binding of C5 to spike protein could also be blocked by ACE2 protein (Figure 2E). Based on the data, we deduced that C5 could be used as a blocker against spike binding to ACE2 to neutralize the virus. Unfortunately, C5 showed no neutralizing activity against SARS-CoV-2 pseudovirus as the IC_{50} was greater than 1000 ng/ml (Figure 4B), probably due to its low binding affinity to RBD (1.80×10^{-8} M) (Figure 2F). In addition, as the protein yield and SEC profile were poor, we sought to engineer C5 by phage display to further improve its affinity and hopefully biophysical properties as well.

Affinity maturation of C5 nanobody by phage display

To increase the binding affinity of nanobody C5 to RBD, we applied a method called "soft randomization" [44] . All the three CDRs of C5 were randomized simultaneously by doped oligos using Kunkel method, resulting in a bias library (See Methods). After four rounds of phage panning, ten C5 variants that specifically bind to RBD were obtained and their three CDRs were multi-aligned (Figure 3A). The multi-alignment result clearly showed the variable residues and the conserved ones in three CDRs. Notably, the variable residues of CDR3 gathered at the end of the loop, i.e. residues 104, 106 and 107. This highly variable region might enable CDR3 evolve extra binding capacity other than the regions at the central part.

As the C5 protein were highly insoluble (data not shown), we expected high yield of protein from those ten C5 variants. Fortunately, we were able to purify variant G2 (hereafter referred to C5G2) with significant increase in yield, i.e. from 0.3mg to 5mg protein per liter culture. The purified C5G2 was above 95% purity as resolved in SDS-PAGE (Figure 3B). The binding affinity of C5G2 to RBD (1.62×10^{-9} M) is ~10 fold higher than the original C5 (Figure 3C), mainly due to the increased K_{dis} rate, which is from 2.59×10^{-4} s^{-1} to 2.84×10^{-5} s^{-1} (Table2). The single peak in the SEC profile of C5G2 also indicated that there was no aggregation in this C5 optimized variant (Figure 3D).

Pseudovirus assay of C5G2 confirmed its broad-spectrum neutralising activities

We then tested if the affinity matured C5G2 could inhibit the binding of RBD to ACE2 and subsequently neutralizing the SARS-CoV-2 pseudovirus infection. We also included D3 nanobody in this study as the negative control as well as mNb6 nanobody [10] as the positive control. We first applied a competitive ELISA assay, in which C5G2 protein and the control proteins were employed to compete with ACE2 binding to RBD. As shown in Figure 4A, with the increase of C5G2 protein concentration, the binding of RBD to ACE2 decreased and the measured IC_{50} was 3.75nM, which was comparable to that of mNb6 (4.64 nM). Meanwhile, the controlled D3 protein, which recognizes a non-RBD epitope, showed no inhibition at all. Based on the data, C5G2 nanobody could interfere with the binding of RBD to ACE2 and the efficient was closed to the reported potent nanobody mNb6.

We then applied pseudovirus assay to test if C5G2 protein could inhibit the infection of pseudovirus to living cells. As shown in Figure 4B, C5G2 could neutralize the WT pseudovirus with a high potency as the IC_{50} is 1.56nM. Meanwhile, the IC_{50} of mNb6 is 13.7 nM. C5G2 is about 9-fold higher potency than mNb6 in this experiment. Surprisingly, C5G2 showed even high potency in neutralizing Alpha, Beta and Gamma variants, with IC_{50} of 0.95 nM, 1.06 nM and 0.56 nM, respectively (Figure 4B). Unfortunately, C5G2 showed no neutralizing efficacy against Delta variant. During the preparation of this manuscript, the Omicron variant emerged and propagate rapidly worldwide. We produced the pseudovirus of Omicron variant and test C5G2's potency in protecting the cells from virus infection. As showed in Figure 4B, C5G2 has an even higher potency as the IC50 of 0.3 nM compared to other VOCs. Taken together, C5G2 showed broad-spectrum neutralizing activities against most of VOCs except for Delta variant.

Structural basis for the broad spectrum neutralization activity of C5G2

To decipher the molecular basis for the neutralization breadth of C5G2, we determined the cryo-electron microscopy (cryo-EM) structure of C5G2 in complex with SARS-CoV-2 S protein at an overall resolution of 3.57 Å (Figure 5A-B, Figure S3 and Table S2). Compared to the wildly reported structure of prefusion spike which have one RBD in open (up) state and the other two in closed (down) state, C5G2 could recognize both the opened and the closed RBDs and the binding of which could induce the transition of one more RBD from down to up state (Figure

5B). Due to its relatively smaller size than conventional IgG antibody (or Fab) and its long CDR3 loop, C5G2 could insert itself into the slit between the RBD and the adjacent NTD and make contact to both the RBD and NTD (Figure 5B). Unfortunately, because of the structural flexibility of the RBD, the interaction details were failed to unveiled in the initial reconstruction. Subsequently, we further performed a local refinement of one C5G2 plus the surrounding RBD and NTD (G5G2: RBD: NTD) at a resolution of 3.88 Å (Figure 5C, Figure S3 and Table S2). Consequently, the high resolution details of local refinement allowed us to build the atomic model of C5G2 and bound RBD and NTD, which confirmed the simultaneous interaction of C5G2 to the RBD and NTD (Figure 5D). C5G2 dominantly interacts with the RBD and results in an extremely large buried area of about 1,160 $Å^2$ on RBD, in contrast, the buried area of the same C5G2 on the NTD is about 200 $Å^2$ (Figure 5D).

C5G2 mainly uses its long CDR3 for meditating the interaction to both the RBD and the NTD (Figure 5E-G). the CDR3 residues F109, H112, N113 and W115 form 5 hydrogen bonds to the RBD (Figure 5E), and residues R104 and N106 form 2 hydrogen bonds and many contact interaction to the NTD (Figure 5G). Of note, the NTD residue N165 and decorated glycan both participate in the interaction to C5G2 (Figure 5G). In addition, the CDR2 of C5G2 also interacts with the RBD and forms additional two hydrogen bonds mediated by the residues Y59 and D62 (Figure 5F). Since it is the RBD that mainly mediated the interaction to C5G2, we next explored the conservation of the C5G2 epitope on RBD. A total of 20 residues (346, 349, 351-356, 449-450, 452, 466, 468, 470-472 and 482-485) on RBD are involved in the interactions to C5G2 (Figure 5H). Of these, 90% (18 residues) are highly conserved among all five variants of concern (VOCs) of Alpha, Beta, Gamma, Delta and Omicron (Figure 5H). Although the epitope residue L452 did not involved in hydrogen bond or salt bridge interactions to C5G2, the L452R mutation on Delta variant will completely abolish the activity of C5G2 (Figure 4B).

Interestingly, C5G2 showed strong inhibition potential against the binding of ACE2 to RBD (Figure 4A). Structurally, although C5G2 recognizes an epitope far away from the binding site of ACE2, the binding of C5G2 will induce steric clashes to the putative ACE2 that bind to the same RBD (Figure S4). Given its high binding affinity, C5G2 would block the binding of ACE2 to RBD by steric hindrance. Furthermore, although the currently dominant Omicron variant holds

unprecedented 15 mutations on its RBD, C5G2 showed effective neutralization potency against Omicron pseudovirus (Figure 4B). Structural analysis showed that, of this 15 mutations, only one (E484A) was found located in the footprint of C5G2 (Figure 5H), suggesting the epitope conservation among SARS-CoV-2 and Omicron variant.

Discussion

Synthetic antibody library is an common and reliable way to obtain antibodies for diagnosis and therapy[10, 35, 45, 46]. In this study, we firstly constructed a universal synthetic nanobody library for the purpose of generating nanobodies for diverse antigens. The library design strategy is straightforward and readily be conducted. Though less sophisticated compared to the reported synthetic libraries [47, 48], the resulting library ASyNAL still enabled us to obtain at least one nanobody for the randomly selected antigens(Table 1), proving its versatile utilization for nanobody generation. The binding affinity of the S protein(and its fragments) nanobodies from the ASyNAL library ranged from 5.58×10^{-10} M to 3.05×10^{-7} M(Table 2), which is within the affinity scope for the synthetic antibodies as well as the natural ones. The SEC profile of the S protein nanobodies indicated that most of the nanobodies have minimal aggregation. Therefore, the the ASyNAL library is a reliable resource of nanobodies with high affinities and good biophysical properties.

It is essential to develop broad-spectrum neutralising antibodies against SARS-CoV-2 as this virus keeps mutating rapidly and becomes more contagious. Luckily, we were able to obtain nanobody C5 by panning ASyNAL library, which could interfere mutually with ACE2 to interact with RBD/Spike. Unfortunately, C5 nanobody didn't show obvious neutralising efficacy against pseudovirus infection, likely due to its relatively low affinity to RBD. Although the binding affinity/avidity of nanobodies could be improved by linking two or more nanobodies together through peptide linker(s) [10, 49, 50], we alternately chose to randomize the three CDRs of C5 to make a phage display library and repeated the panning by increase the selection stringency(see Methonds). Consequently, we obtained variant C5G2 with more than 10-fold increase in binding affinity(1.6 nM) to RBD yet keeping the blocking capacity against ACE2(Figure 4A). In addition, C5G2 could interact with most RBD domains from the major variant of concern in ELISA assay, which implies it has broad neutralising activity against different virus variants. We purified the C5G2 protein as monovalent nanobody for pseudovirus

assay. As expected, C5G2 protected cells from WT pseudovirus infection potently with single digital nanomolar IC_{50} value, verifying its neutralising capacity.
Additionally, C5G2 could inhibit the infection of most of the virus of concern(VOC), especially Omicron variant in the pseudovirus assay with similar or higher potency, implying its broad spectrum neutralising capacity. C5G2 is one of the few reported broad-spectrum antibodies so far[51-53] that neutralize Omicron variant in addition to the wild type virus. In terms of the potency(i.e. IC50 in pseudovirus assay), the monovalent C5G2 is comparable to the newly FDA approved drug(bebtelovimab) for COVID-19 that retains activity against Omicron variant. To our best, C5G2 is the first nanobody to date that has high potency against Omicron variant even in its monovalent format. We also predict that it is highly likely that multivalent format of C5G2, which benefit from the avidity, could drive the neutralising potency even higher.

To decipher the molecular mechanism of C5G2's activity, we solved the Cryo-EM structure of C5G2 in complex with the trimer of Spike protein. The structure showed that C5G2 made extensive contact with RBD mainly through its CDR3 loop by binding to a surface that is distinct from that of ACE2 binding. That binding surface is relatively conserved among the SARS-CoV-2 variants, which explains why C5G2 is resistant to most of the RBD mutations in the virus variants. Surprisingly, C5G2 made further contact with adjacent NTD through the end of its CDR3 loop, which makes it bind two distinct epitopes simultaneously in one spike trimer . Based on the solved structure in this study, the C5G2 binding residues in RBD and NTD are highly conservative among SARS-CoV-2 variant virus [54], which may be the main cause that it behaves a broad spectrum neutralising nanobody in the pseudovirus assay.

Furthermore, it was an accident that we obtained the extra NTD binding capacity of C5G2 during the affinity maturation process. Bi-paratopic antibodies are usually developed by linking two antibodies together[55] or be engineered from a conventional Fab as it has enough binding surface formed by six CDRs [56] . To our best knowledge, C5G2 is the first reported monovalent bi-paratopic nanobody to date, which binds to its two epitopes through one CDR3. We predict that by engineering the NTD binding paratope, i.e. the residues R104, N106 etc. of CDR3 loop of

C5G2 it would increase the binding affinity of C5G2 to spike protein, which may drive the neutralising potency of C5G2 even higher. Based on the C5G2's binding property in this study, it is also likely to develop bi-paratopic nanobody targeting two epitopes in two different antigens in the future due to the long CDR3 loops of most nanobodies.

Taken together, we expected the methodology provided in this study, from library construction to antibody engineering, could be applied to antibody discovery for other disease-related antigens. By this method, we were able to identify C5G2 nanobody with high potency and broad-spectrum neutralising activity against SARS-CoV-2 virus and most of its popular variants. There're many advantages of nanobodies, such as high affinities to their antigens, facile expression in E. coli system, etc. Due to the small size of C5G2(15kD), high potency in the monovalent format and broad-spectrum activity, it may be developed as inhale drug that play a role in the prophylaxis and therapy of the COVID-19 caused by SARS-CoV-2 virus and its emerging and future variants.

Materials and Methods

Construction of a synthetic nanobody library

In order to construct a novel synthetic nanobody library, a natural nanobody (PDB no. 1ZVH) from camel that recognizes lysozyme was used as template for mutagenesis. The coding cDNA of 1ZVH was chemically synthesized and subcloned into a modified phage display vector of pComb3XSS, in which the amber stop codon (TAG) were mutated to CAG to facilitate nanobody display in *E. coli* without gene supE, e.g. SS320(Genentech). The 1ZVH construct was firstly transformed into *E. coli* SS320 and the phage were produced by adding helper phage M13KO7 (New England Biolabs). The successful display of 1ZVH was then verified by phage ELISA, in which the produced phage could be bound by immobilized lysozyme in a 96-well NUNC Maxisorp plate.

To increase the oligo incorporation efficiency, two ochre stop codon (TAA) and one BamH I restriction enzyme site (GGATCC) in between were applied to replace the CDR3 region of 1ZVH to generate a so called "Stop template". The "Stop template" was transformed into *E. coli* CJ236 (New England Biolabs) to produce *du* single strand DNA (*du*-ssDNA) as described previously[57]. The mutation strategy was using degenerate oligo mix (X) to incorporate into the CDR1 (7aa), CDR2 (8aa) and CDR3 (14aa) of the 1ZVH, respectively (Figure 1A). The degenerate oligo mix X denotes 16% of Tyrosine, 10% of Glycing, 10% Serine, 5% of Alanine, Aspartate, Glutamate, Phenylalanine, Histidine, Isoleucine, Lysine, Leucine, Glutamine, Arginine, Threonine, and Valine, respectively and 1% of Methionine, Asparagine and Tryptophan, respectively. The oligos for each CDR were synthesized by a TRIMER-like method by Genewiz (Suzhou, China). The CDR oligos were incorporated into the corresponding CDR regions simultaneously by standard Kunkel reaction as described previously[43]. The Kunkel product was transformed into 350 µL high efficiency competent cell SS320 (with M13KO7 incorporated) made by electroporation as described previously [43]. The transformed SS320 were grown overnight in 2YT media supplemented with 50 µg/mL carbenicillin at 32°C with a shaking speed of 200 rpm. To increase the incorporation percentage at CDR3 region, the SS320 cells were pelleted and the the plasmid DNA were maxipreped. 20 µg plasmid DNA were digested by restriction enzyme BamH I to

remove those DNA molecules with failed incorporation at CDR3 region (i.e. the Stop templates) for at least 4 hours at 37°C. The resultant DNA were purified in a PCR product purification column to remove ions and enzymes. The DNA sample were re-suspended into a minimum volume, i.e. 60µL H_2O. The digested DNA sample was re-transformed into 350 µL competent cell SS320 (+M13KO7) by electroporation. The transformed SS320 cells were grown as above and the phages in the supernatant were precipitated by PEG/NaCl (20%/2.5M). The concentration of the phage solution was determined by serial dilution and by infection of XL1-Blue (Stratagene) as described previously[43].

Library quality control by next generation sequencing

The library DNA were applied as templates in PCR reaction and the nanobody encoding sequences were amplified by Phanta Max Super-Fidelity DNA Polymerase (Vazyme). The PCR products were resolved in 1.5% agrose gel and the band was sliced for gel purification. The purified DNA were subject for Next generation sequencing (NGS). More than 50 ng purified PCR fragments were used for library preparation. These PCR products were treated with End Prep Enzyme Mix for end repairing, 5' Phosphorylation and dA-tailing in one reaction, followed by a T-A ligation to add adaptors to both ends. Adaptor-ligated DNA was then performed using DNA Clean Beads. A second PCR reaction was carried out with two primers carrying sequences which can anneal with flowcell to perform bridge PCR and index allowing for multiplexing. The final library product for sequencing were then purified by beads and was qualified. The qualified libraries were sequenced pair end 150 bp on Illumina NovaSeq 6000. The method of data analysis is performed as described previously [43].

Phage biopanning

The phage biopanning was performed as previously described [58]. Briefly, Two wells of 96-well microplate (NUNC) were coated with 0.5 µg antigen (e.g. RBD-Fc or other antigens) and 0.5µg Fc in 100µL 1×PBS (137 mM NaCl, 3 mM KCl, 8mM Na_2HPO_4 and 1.5mM KH_2PO_4, pH=7.6) overnight, respectively. Solution in the well were discarded and 200 µL/well 2% skim milk were added for blocking at room temperature for 1 hour. After incubation, solution were discarded

and 100 µL/well phage-displayed nanobody library (~3.0×10^{12} phage clones, approximately 1000× library diversity) were added to the Fc wells for pre-incubation to remove the non-specific binders. After incubation at room temperature for 1 hour, phage solution were then transferred into the RBD-Fc well for binding for 1 hour. Non-binding phages were washed away by PT buffer (1×PBS + 0.05% Tween) for at least 8 times. Bound phages were eluted by 100mM HCl 100 µL/well. 1/8 volume of Tris-HCl (1M, pH=11) were then added for neutralization. Half volume of the neutralized phage solution was then applied to infect 10-fold volume of actively growing *E. coli* XL1-blue (Stratagene) for 30 min at 37 ℃. Then M13KO7 helper phages (NEB, N0315S) were added at a final concentration of 1×10^{10} phages/mL for super infection for 45 min. The XL1-blue culture was added into 20-fold volume of 2YT medium (10 g yeast extract, 16 g tryptone, 5 g NaCl in 1L water) supplemented with Carb (carbenicillin, 50 mg/µL) and Kana (kanamycin, 25 mg/µL), and grow overnight (14-16 hours) at 32℃, 200 rpm in a shaker. The overnight culture was centrifuged and the supernatant were precipitated by 1/5 volume of PEG/NaCl (20% PEG 8000/2.5M NaCl). The amplified phage in the pellets were resuspend with 1mL 1×PBS and applied as the input phage for the next round of panning. For C5 variant library panning, from the second round, antigen RBD-Fc were decreased from 0.5µg to 0.2µg (2nd round), 0.1µg (3rd round), 0.05µg (4th round) to increase the selection stringency.

Phage ELISA

In a 96-well NUNC microplate, 0.1 µg /well RBD-Fc (or other antigens) and 0.1 µg /well Fc were coated in wells in 50µL 1×PBS, respectively. After incubation at 4℃ overnight, solution in the well was discarded and 100 µL/well 2% milk were added for blocking at room temperature for 1 hour. 2×50µL phage solution were added into the RBD-Fc wells and Fc wells, respectively, for binding for 1 hour. Non-binding phage were washed away 8 times by PT buffer. 50µL anti-M13/HRP conjugate (Sino Biological) were added and incubated for 30 min. After wash by PT buffer, 50µL TMB substrate were add to develop color according to the manufacturer's instruction. 100 µL of 1.0 M H_3PO_4 were added to stop the reaction and signals were read

spectrophotometrically at 450 nm in a BioTek plate reader. The reads of RBD-Fc and Fc wells were recorded and the ratio of RBD-Fc/ Fc were calculated.

Competitive phage ELISA:

0.2 ug/well Spike-trimer-His (Acrobiosystem) /RBD-Fc were coated in microplate in 50uL 1×PBS buffer at 4℃ overnight. 100 µL/well 2% milk were incubated for 1 hour for blocking. After washing for 3 times, a serial phage solution was added to incubate with spike-trimer-His for 30 minutes. Anti-M13/HRP conjugate (1:8000 dilution) and TMB were used to amplify the signals and develop color reaction, respectively. After stopping reaction via 1.0 M H_3PO_4, OD 450 value was read by microplate reader. After that, subsaturation (80% of maximal effect) concentration of phage solution was used for competitive Elisa.

0.2 ug/well Spike-trimer-His/RBD-Fc were coated for competitive phage Elisa. After incubation with 100 uL/well 2% milk for 1 hour and 3 times washing, subsaturation concentration of phage solution mixed with decreased concentration of ACE2-Fc (Novoprotein). The mixture of phage and ACE2-Fc was added to wells coated with Spike-trimer-His/RBD-Fc and incubation for 30 minutes. M13/HRP conjugate, TMB, 1.0 M H_3PO_4 and microplate reader were used for subsequent operation as described above.

C5 affinity maturation library construction

The sequence of C5 in phagemid pComb3XSS were used as template for library construction. The C5 du-ssDNA used for Kunkel reaction was made as described previously [57]. Primer 1 (AGCTGTGCAGCAAGTGGA*TAAGGATCCTAA*CTAGGCTGGTTTCGTCAA), Primer 2 (CGCGAAGGAGTTGCTGCA*TAAGGATCCTAA*TACTACGCCGATAGCGTG), and Primer 3 (CTGTACTATTGTGCGGCC*TAAGGATCCTAA*AACTACTGGGGCCAAGGC) were used in a combinatorial reaction by Kunkel method to construct a “Stop template”, in which all CDRs were incorporated with BamH I restriction enzyme recognition site *GGATCC* and two stop codons *TAA*. Then Primer 4 (AGCTGTGCAGCAAGTGGA$N_1N_1N_1N_2N_1N_2N_1N_4N_3N_3N_1N_2N_3N_2N_4N_4N_4N_2N_2N_2N_2$CTAGGCTGGTTTCGTCAA),

Primer 5 (CGCGAAGGAGTTGCTGCA$N_4N_4N_2N_3N_2N_4N_4N_4N_2N_4N_3N_1N_2N_1N_2N_4N_1N_1N_4N_1N_2N_4N_4N_2$TACTACGCCGATAGCGTG) and Primer 6 (CTGTACTATTGTGCGGCC$N_3N_2N_4N_4N_2N_2N_4N_2N_2N_2N_2N_2N_1N_4N_3N_3N_4N_2N_4N_1N_2N_1N_4N_3N_3N_3N_4N_4N_1N_1N_2N_2N_2N_3N_2N_4N_4N_3N_1N_3N_1N_4$AACTACTGGGGCCAAGGC) were applied simultaneously in a Kunkel method to synthesize the heteroduplex double strand DNA (dsDNA), in which the designed mutations at each position were incorporate into the "Stop template". In the above primers, N_1 is composed of the mixture of 85% of A, 5% of G, T and C, respectively; N_2 represents the mixture of 85% of T and 5% of A, G and C; N_3 means the mixture of 85% of C, 5% of A, T and G; N_4 contains 85% of G, 5% of T, A and C. The dsDNA was further digested by restriction enzymes BamH I to remove the unreacted template molecules before transformed into *E. coli* SS320 (pre-infected by M13KO7) by electroporation. The transformation efficiency (library diversity) was calculated by bacterial serial dilution as described [58]. The resulting phage library was precipitated by PEG/NaCl (20% PEG 8000/2.5M NaCl) as described[43].

Nanobody expression and purification

The cDNA encoding the nanobodies in the pComb3XSS vector were PCR amplified and subcloned into vector pET22b to express 6×His tagged proteins. The expression constructs were transformed in to *E. coli* BL21 (DE3). Single colonies were picked and grow in 2YT/Carb medium at 37℃ to OD_{600}=0.8. IPTG were added to a final concentration of 0.2 mM and protein expression was induced at 18 ℃ overnight. The culture was centrifuged and the pellets were treated as previously described [59]. Briefly, pellets were re-suspended in lysis buffer (to make 100 mL lysis buffer: 98 mL Hepes/NaCl (50 mM/500mM) buffer, 1 mL TritonX-100, 1 mL 100× protease inhibitor cocktail, 10 µL benzonase, 5% glycerol, 100 mg lysozyme). Both the lysate and the supernatant from the overnight were heated at 60℃ for 30 min to denature partially folded nanobodies. Heat-treated lysate and supernatant were centrifuged again and subjected for antibody purification. Antibody were purified using Ni-NTA agrose (Qiagen) according to the manufacturer's manual. The eluted proteins were buffer exchanged into 1×PBS by Amicon

Ultra-4 Centrifugal Filter Units (Millipore). The final concentrations of the proteins were determined by BCA method. The purity of the nanobodies were resolved in 15% SDS-PAGE gels.

Competitive protein ELISA

In a 96-well NUNC microplate, 0.2 μg ACE2-His (Novoprotein) were coated per well in 50 μL 1×PBS at 4℃ overnight. Then 100 μL/well 2% milk were added for blocking for 1 hour. A serial RBD-Fc with increased concentration (0nM, 3.125nM, 6.25nM…100nM, 200nM) were added in 9 wells coated with ACE2-His. The wells were washed 5 times by PT buffer after incubation for 1 hour at room temperature. 50 μL of Anti-IgG-HRP conjugate (Shanghai Ruian) were added to each well and incubated for 30 min. After washing 8 times by PT buffer, 50μL TMB substrate were add to develop color for 2 min. 100 μL of 1.0 M H_3PO_4 were added to stop the reaction and signals were read spectrophotometrically at 450 nm in a plate reader. Standard variation values were calculated using a 3-parameter logistic regression fit using Prism Software (GraphPad). Concentration for 80% of maximal effect (the sub-saturation concentration) were applied for the following competitive ELISA. 0.2μg/well ACE2-His were coated in a 96-well NUNC microplate. After incubation at 4 ℃ overnight, 100 μL/well 2% milk were used for blocking. Sub-saturation concentration of RBD-Fc were mixed with a serial nanobody-His with decreased concentration (500nM, 250nM, 125nM… 0nM). The mixture was added to 12 wells coated with ACE2-His and incubated at room temperature for 30 mins. After incubation with Anti-IgG-HRP and washed by PT buffer, TMB were used to develop color. The reaction was terminated with 1.0 M H_3PO_4 and the OD_{450} value was read through a Biotek Microplate Reader. Each reaction was triplicated and the mean of the readout were used for IC_{50} calculation.

Size-exclusion chromatography

The buffer of nanobody was changed to 1×PBS (PH=7.4) by ultrafiltration discs (Merck, PLBC07610). 50μL nanobody (1 mg/mL) were filtered through a 0.2 μm filter. After that, filtered samples were prepared for HPLC analysis. HPLC instrument (Waters, ACQUITY UPLC H-Clas) was

used to purity analysis of proteins. PBS and the gel permeation chromatography column (TSKgel G3000SW$_{XL}$,Tosoh Bioscience, 0008541) were used as the mobile phase and the stationary phase, respectively. The pump was running for 5 minutes, mainly to eliminate air bubbles in the system, and then closed all exhaust valves. The mobile phase was running at a fixed rate(1mL/min) until the baseline is stable. Then, the operating parameters(Flow rate: 1 mL/min, pressure: 3.3MPa, temperature: 25℃, detection: UV 280nm) of sample was set in the software (Waters, Empower3). After that, sample was injected into the sampling valve and the line was monitored by software. The sample was allowed to run for 20 min (more than 1.5×column volume) before stopped.

Bio-layer interferometry (BLI) assay

BLI experiments were carried out using an Octet RED96 System (ForteBio). The measurements were performed using Ni-NTA biosensors (ForteBio). The nanobodies with 6×His tag were immobilized on the biosensor tip surface. All steps were performed at 30℃ with shaking at 1000 rpm in a black 96-well plate, with a working volume of 200 µL in each well.
The RBD-Fc with different concentration (250nM, 125nM, 0nM) in the running buffer (1×PBS + 0.5% BSA + 0.05% Tween) was applied for association and dissociation. The response data were normalized using Octet data analysis software version 9.0.0.14 (ForteBio).

Pseudovirus-based neutralization assay

Vesicular stomatitis virus (VSV) dG-SARS-Cov2 virus were used as pseudovirus and BHK21-hACE2 were prepared for neutralization assay [60]. Gradient diluted nanobodies were added to VSV dG-SARS-Cov2 virus (MOI=0.05) then incubated at 37℃ for 1h. All samples and virus were diluted by 10% FBS-DMEM. After incubation, mixture were added to BHK21-hACE2 and incubated for 12h. Fluorescence images were obtained with Opera Phenix or Operetta CLS equipment (PerkinElmer) and analyzed by the Columbus system (PerkinElmer). Compare the number of GFP-positive cells in nanobody treated group and in nontreated group to calculate the reduction ratio which represents the neutralizing potency.

Cryo-EM sample and data collection

Aliquots (3 µL) of 3.5 mg/mL mixtures of purified SARS-CoV-2 S protein (Acrobiosystem) in complex with excess C5G2 of three nAbs were incubated in 0.01% (v/v) Digitonin (Sigma) and then loaded onto glow-discharged (60 s at 20 mA) holey carbon Quantifoil grids (R1.2/1.3, 200 mesh, Quantifoil Micro Tools) using a Vitrobot Mark IV (ThermoFisher Scientific) at 100% humidity and 4°C. Data were acquired using the SerialEM software on an FEI Tecnai F30 transmission electron microscope (ThermoFisher Scientific) operated at 300 kV and equipped with a Gatan K3 direct detector. Images were recorded in the 36-frame movie mode at a nominal 39,000× magnification at super-resolution mode with a pixel size of 0.389 Å. The total electron dose was set to 60 e^{-} $Å^{-2}$ and the exposure time was 4.5 s.

Image processing and 3D reconstruction

Drift and beam-induced motion correction were performed with MotionCor2 [61] to produce a micrograph from each movie. Contrast transfer function (CTF) fitting and phase-shift estimation were conducted with Gctf [62]. Micrographs with astigmatism, obvious drift, or contamination were discarded before reconstruction. The following reconstruction procedures were performed by using Cryosparc V3 [63]. In brief, particles were automatically picked by using the "Blob picker" or "Template picker". Several rounds of reference-free 2D classifications were performed and the selected good particles were then subjected to ab-initio reconstruction, heterogeneous refinement and final non-uniform refinement. The resolution of all density maps was determined by the gold-standard Fourier shell correlation curve, with a cutoff of 0.143 [64]. Local map resolution was estimated with ResMap [65].

Atomic model building, refinement, and 3D visualization

The initial model of nAbs was generated from homology modeling by Accelrys Discovery Studio software (available from: URL: https://www.3dsbiovia.com). The structure of SARS-CoV-2 RBD from the structure of WT trimeric spike (pdb no. 6VSB[66]) was used as the initial modes of our WT-RBD. We initially fitted the templates models into the corresponding final cryo-EM map

using Chimera [67], and further corrected and adjusted them manually by real-space refinement in Coot [68]. The resulting models were then refined with phenix.real_space_refine in PHENIX [69]. These operations were executed iteratively until the problematic regions, Ramachandran outliers, and poor rotamers were either eliminated or moved to favored regions. The final atomic models were validated with Molprobity [70, 71]. All figures were generated with Chimera or ChimeraX [72, 73].

Conflict of Interest

D.Z. was an intern of Noventi Biopharmaceuticals Co., Ltd. Y.Y., L.L., D.J., and H.H. are the employees of Noventi Biopharmaceuticals Co., Ltd. X.Y. is the employee of Guangxi Asia United Antibody Medical Co., Ltd.

Reference

1. Chan, J.F., et al., *A familial cluster of pneumonia associated with the 2019 novel coronavirus indicating person-to-person transmission: a study of a family cluster.* Lancet, 2020. **395**(10223): p. 514-523.
2. Huang, C., et al., *Clinical features of patients infected with 2019 novel coronavirus in Wuhan, China.* Lancet, 2020. **395**(10223): p. 497-506.
3. Zhou, P., et al., *A pneumonia outbreak associated with a new coronavirus of probable bat origin.* Nature, 2020. **579**(7798): p. 270-273.
4. Walls, A.C., et al., *Structure, Function, and Antigenicity of the SARS-CoV-2 Spike Glycoprotein.* Cell, 2020. **181**(2): p. 281-292 e6.
5. Huang, Y., et al., *Structural and functional properties of SARS-CoV-2 spike protein: potential antivirus drug development for COVID-19.* Acta Pharmacol Sin, 2020. **41**(9): p. 1141-1149.
6. Hoffmann, M., H. Kleine-Weber, and S. Pohlmann, *A Multibasic Cleavage Site in the Spike Protein of SARS-CoV-2 Is Essential for Infection of Human Lung Cells.* Mol Cell, 2020. **78**(4): p. 779-784 e5.
7. Xia, X., *Domains and Functions of Spike Protein in Sars-Cov-2 in the Context of Vaccine Design.* Viruses, 2021. **13**(1).
8. Xia, S., et al., *Fusion mechanism of 2019-nCoV and fusion inhibitors targeting HR1 domain in spike protein.* Cell Mol Immunol, 2020. **17**(7): p. 765-767.
9. Hoffmann, M., et al., *SARS-CoV-2 Cell Entry Depends on ACE2 and TMPRSS2 and Is Blocked by a Clinically Proven Protease Inhibitor.* Cell, 2020. **181**(2): p. 271-280 e8.
10. Schoof, M., et al., *An ultrapotent synthetic nanobody neutralizes SARS-CoV-2 by stabilizing inactive Spike.* Science, 2020. **370**(6523): p. 1473-1479.

11. Koenig, P.A., et al., *Structure-guided multivalent nanobodies block SARS-CoV-2 infection and suppress mutational escape.* Science, 2021. **371**(6530).
12. Chen, W.H., et al., *Yeast-expressed recombinant SARS-CoV-2 receptor binding domain RBD203-N1 as a COVID-19 protein vaccine candidate.* Protein Expr Purif, 2022. **190**: p. 106003.
13. Dagotto, G., J. Yu, and D.H. Barouch, *Approaches and Challenges in SARS-CoV-2 Vaccine Development.* Cell Host Microbe, 2020. **28**(3): p. 364-370.
14. Rawat, K., P. Kumari, and L. Saha, *COVID-19 vaccine: A recent update in pipeline vaccines, their design and development strategies.* Eur J Pharmacol, 2021. **892**: p. 173751.
15. Xiang, Y., et al., *Versatile and multivalent nanobodies efficiently neutralize SARS-CoV-2.* Science, 2020. **370**(6523): p. 1479-1484.
16. Xu, J., et al., *Nanobodies from camelid mice and llamas neutralize SARS-CoV-2 variants.* Nature, 2021. **595**(7866): p. 278-282.
17. Chi, X., et al., *A neutralizing human antibody binds to the N-terminal domain of the Spike protein of SARS-CoV-2.* Science, 2020. **369**(6504): p. 650-655.
18. Liu, L., et al., *Potent neutralizing antibodies against multiple epitopes on SARS-CoV-2 spike.* Nature, 2020. **584**(7821): p. 450-456.
19. Tang, Q., R.J. Owens, and J.H. Naismith, *Structural Biology of Nanobodies against the Spike Protein of SARS-CoV-2.* Viruses, 2021. **13**(11).
20. Huo, J., et al., *Neutralizing nanobodies bind SARS-CoV-2 spike RBD and block interaction with ACE2.* Nat Struct Mol Biol, 2020. **27**(9): p. 846-854.
21. Hansen, J., et al., *Studies in humanized mice and convalescent humans yield a SARS-CoV-2 antibody cocktail.* Science, 2020. **369**(6506): p. 1010-1014.
22. Kreye, J., et al., *A SARS-CoV-2 neutralizing antibody protects from lung pathology in a COVID-19 hamster model.* bioRxiv, 2020.
23. Shi, R., et al., *A human neutralizing antibody targets the receptor-binding site of SARS-CoV-2.* Nature, 2020. **584**(7819): p. 120-124.
24. Huo, J., et al., *Neutralization of SARS-CoV-2 by Destruction of the Prefusion Spike.* Cell Host Microbe, 2020. **28**(3): p. 445-454 e6.
25. Pinto, D., et al., *Cross-neutralization of SARS-CoV-2 by a human monoclonal SARS-CoV antibody.* Nature, 2020. **583**(7815): p. 290-295.
26. Cao, Y., et al., *Potent Neutralizing Antibodies against SARS-CoV-2 Identified by High-Throughput Single-Cell Sequencing of Convalescent Patients' B Cells.* Cell, 2020. **182**(1): p. 73-84 e16.
27. Ju, B., et al., *Human neutralizing antibodies elicited by SARS-CoV-2 infection.* Nature, 2020. **584**(7819): p. 115-119.
28. Adams, J.J. and S.S. Sidhu, *Synthetic antibody technologies.* Curr Opin Struct Biol, 2014. **24**: p. 1-9.
29. Shim, H., *Synthetic approach to the generation of antibody diversity.* BMB Rep, 2015. **48**(9): p. 489-94.
30. Yang, H.Y., et al., *Construction of a large synthetic human scFv library with six diversified CDRs and high functional diversity.* Mol Cells, 2009. **27**(2): p. 225-35.

31. Boehncke, W.H., N.C. Brembilla, and M.J. Nissen, *Guselkumab: the First Selective IL-23 Inhibitor for Active Psoriatic Arthritis in Adults.* Expert Rev Clin Immunol, 2021. **17**(1): p. 5-13.
32. Blauvelt, A., et al., *Efficacy and safety of guselkumab, an anti-interleukin-23 monoclonal antibody, compared with adalimumab for the continuous treatment of patients with moderate to severe psoriasis: Results from the phase III, double-blinded, placebo- and active comparator-controlled VOYAGE 1 trial.* J Am Acad Dermatol, 2017. **76**(3): p. 405-417.
33. Reich, K., et al., *Efficacy and safety of guselkumab, an anti-interleukin-23 monoclonal antibody, compared with adalimumab for the treatment of patients with moderate to severe psoriasis with randomized withdrawal and retreatment: Results from the phase III, double-blind, placebo- and active comparator-controlled VOYAGE 2 trial.* J Am Acad Dermatol, 2017. **76**(3): p. 418-431.
34. Deodhar, A., et al., *Guselkumab in patients with active psoriatic arthritis who were biologic-naive or had previously received TNFalpha inhibitor treatment (DISCOVER-1): a double-blind, randomised, placebo-controlled phase 3 trial.* Lancet, 2020. **395**(10230): p. 1115-1125.
35. Knappik, A., et al., *Fully synthetic human combinatorial antibody libraries (HuCAL) based on modular consensus frameworks and CDRs randomized with trinucleotides.* J Mol Biol, 2000. **296**(1): p. 57-86.
36. Muyldermans, S., *Nanobodies: natural single-domain antibodies.* Annu Rev Biochem, 2013. **82**: p. 775-97.
37. Gonzalez-Sapienza, G., M.A. Rossotti, and S. Tabares-da Rosa, *Single-Domain Antibodies As Versatile Affinity Reagents for Analytical and Diagnostic Applications.* Front Immunol, 2017. **8**: p. 977.
38. Muyldermans, S., *Single domain camel antibodies: current status.* J Biotechnol, 2001. **74**(4): p. 277-302.
39. Huo, J., et al., *A potent SARS-CoV-2 neutralising nanobody shows therapeutic efficacy in the Syrian golden hamster model of COVID-19.* Nat Commun, 2021. **12**(1): p. 5469.
40. Wu, Y., et al., *Identification of Human Single-Domain Antibodies against SARS-CoV-2.* Cell Host Microbe, 2020. **27**(6): p. 891-898 e5.
41. De Genst, E., et al., *Molecular basis for the preferential cleft recognition by dromedary heavy-chain antibodies.* Proc Natl Acad Sci U S A, 2006. **103**(12): p. 4586-91.
42. Kunkel, T.A., K. Bebenek, and J. McClary, *Efficient site-directed mutagenesis using uracil-containing DNA.* Methods Enzymol, 1991. **204**: p. 125-39.
43. Li, S., et al., *Revisiting the phosphotyrosine binding pocket of Fyn SH2 domain led to the identification of novel SH2 superbinders.* Protein Sci, 2021. **30**(3): p. 558-570.
44. Kaneko, T., et al., *Superbinder SH2 domains act as antagonists of cell signaling.* Sci Signal, 2012. **5**(243): p. ra68.
45. Custodio, T.F., et al., *Selection, biophysical and structural analysis of synthetic nanobodies that effectively neutralize SARS-CoV-2.* Nat Commun, 2020. **11**(1): p. 5588.
46. Li, T., et al., *A synthetic nanobody targeting RBD protects hamsters from SARS-CoV-2 infection.* Nat Commun, 2021. **12**(1): p. 4635.

47. Moutel, S., et al., *NaLi-H1: A universal synthetic library of humanized nanobodies providing highly functional antibodies and intrabodies.* Elife, 2016. **5**.
48. Zimmermann, I., et al., *Synthetic single domain antibodies for the conformational trapping of membrane proteins.* Elife, 2018. **7**.
49. Bracken, C.J., et al., *Bi-paratopic and multivalent VH domains block ACE2 binding and neutralize SARS-CoV-2.* Nat Chem Biol, 2021. **17**(1): p. 113-121.
50. Lu, Q., et al., *Development of multivalent nanobodies blocking SARS-CoV-2 infection by targeting RBD of spike protein.* J Nanobiotechnology, 2021. **19**(1): p. 33.
51. Westendorf, K., et al., *LY-CoV1404 (bebtelovimab) potently neutralizes SARS-CoV-2 variants.* bioRxiv, 2022.
52. VanBlargan, L., et al., *An infectious SARS-CoV-2 B.1.1.529 Omicron virus escapes neutralization by therapeutic monoclonal antibodies.* Res Sq, 2021.
53. Yin, W., et al., *Structures of the Omicron spike trimer with ACE2 and an anti-Omicron antibody.* Science, 2022. **375**(6584): p. 1048-1053.
54. Harvey, W.T., et al., *SARS-CoV-2 variants, spike mutations and immune escape.* Nat Rev Microbiol, 2021. **19**(7): p. 409-424.
55. Li, J.Y., et al., *A Biparatopic HER2-Targeting Antibody-Drug Conjugate Induces Tumor Regression in Primary Models Refractory to or Ineligible for HER2-Targeted Therapy.* Cancer Cell, 2016. **29**(1): p. 117-29.
56. Bostrom, J., et al., *Variants of the antibody herceptin that interact with HER2 and VEGF at the antigen binding site.* Science, 2009. **323**(5921): p. 1610-4.
57. Tonikian, R., et al., *Identifying specificity profiles for peptide recognition modules from phage-displayed peptide libraries.* Nat Protoc, 2007. **2**(6): p. 1368-86.
58. Huang, H., et al., *Creation of Phosphotyrosine Superbinders by Directed Evolution of an SH2 Domain.* Methods Mol Biol, 2017. **1555**: p. 225-254.
59. Zhong, N., et al., *Optimizing Production of Antigens and Fabs in the Context of Generating Recombinant Antibodies to Human Proteins.* PLoS One, 2015. **10**(10): p. e0139695.
60. Xiong, H.L., et al., *Robust neutralization assay based on SARS-CoV-2 S-protein-bearing vesicular stomatitis virus (VSV) pseudovirus and ACE2-overexpressing BHK21 cells.* Emerg Microbes Infect, 2020. **9**(1): p. 2105-2113.
61. Zheng, S.Q., et al., *MotionCor2: anisotropic correction of beam-induced motion for improved cryo-electron microscopy.* Nat Methods, 2017. **14**(4): p. 331-332.
62. Zhang, K., *Gctf: Real-time CTF determination and correction.* J Struct Biol, 2016. **193**(1): p. 1-12.
63. Punjani, A., et al., *cryoSPARC: algorithms for rapid unsupervised cryo-EM structure determination.* Nat Methods, 2017. **14**(3): p. 290-296.
64. Scheres, S.H. and S. Chen, *Prevention of overfitting in cryo-EM structure determination.* Nat Methods, 2012. **9**(9): p. 853-4.
65. Kucukelbir, A., F.J. Sigworth, and H.D. Tagare, *Quantifying the local resolution of cryo-EM density maps.* Nat Methods, 2014. **11**(1): p. 63-5.
66. Wrapp, D., et al., *Cryo-EM structure of the 2019-nCoV spike in the prefusion conformation.* Science, 2020. **367**(6483): p. 1260-1263.

67. Pettersen, E.F., et al., *UCSF Chimera--a visualization system for exploratory research and analysis.* J Comput Chem, 2004. **25**(13): p. 1605-12.
68. Emsley, P. and K. Cowtan, *Coot: model-building tools for molecular graphics.* Acta Crystallogr D Biol Crystallogr, 2004. **60**(Pt 12 Pt 1): p. 2126-32.
69. Adams, P.D., et al., *PHENIX: a comprehensive Python-based system for macromolecular structure solution.* Acta Crystallogr D Biol Crystallogr, 2010. **66**(Pt 2): p. 213-21.
70. Chen, V.B., et al., *MolProbity: all-atom structure validation for macromolecular crystallography.* Acta Crystallogr D Biol Crystallogr, 2010. **66**(Pt 1): p. 12-21.
71. Robert, X. and P. Gouet, *Deciphering key features in protein structures with the new ENDscript server.* Nucleic Acids Res, 2014. **42**(Web Server issue): p. W320-4.
72. Goddard, T.D., et al., *UCSF ChimeraX: Meeting modern challenges in visualization and analysis.* Protein Sci, 2018. **27**(1): p. 14-25.
73. Pettersen, E.F., et al., *UCSF ChimeraX: Structure visualization for researchers, educators, and developers.* Protein Sci, 2021. **30**(1): p. 70-82.

Table 1 Antigens and their nanobodies selected from ASyNAL library

Antigen	Unique Nb	Category
Lysozyme	10	Secreted enzyme
Fyn SH2	1	Cytoplasmic protein
GST	6	Cytoplasmic protein
Her2	9	Extracellular domain of membrane
Siglec 15	11	Extracellular domain of membrane
SARS-CoV-2 spike	7	Virus protein
Swine Pcv-2d	8	Virus protein

Table2 Anti-Spike nanobody affinity and neutralization potency

Nb	Ag	Spike binding			S1 binding			RBD binding			Pseudovirus IC50(M)					
		KD (M)	Kon(1/Ms)	Kdis(1/s)	KD (M)	Kon(1/Ms)	Kdis(1/s)	KD (M)	Kon(1/Ms)	Kdis(1/s)	Wild type	B.1.1.7 (Alpha)	P.1 (Beta)	B.1.351 (Gamma)	B.1.617.2 (Delta)	B.1.1.529 (Omicron)
B7	RBD							2.66E-07	2.59E+05	6.87E-02						
A11/D3	S1/S				5.58E-10	8.83E+05	4.93E-04				N.E.	N.E.	N.E.	N.E.	N.E.	N.E.
D8	S	3.05E-08	7.71E+04	2.35E-03												
D9	S	2.61E-07	1.87E+05	4.87E-02												
F12	S	1.46E-07	2.51E+05	3.66E-02												
G6	S	2.48E-07	1.40E+05	3.46E-02												
C5	S							1.80E-08	1.44E+04	2.59E-04	N.E.	N.E.	8.16 E-08	N.E.	N.E.	2.1E-09
C5G2	S							1.62E-09	1.76E+04	2.84E-05	1.56E-09	9.5 E-10	5.6 E-10	1.06E-09	N.E.	3.0E-10
mNb6	S							3.48E-09	1.63E+04	5.66E-05	1.37E-08	2.69 E-08	N.E.	N.E.	2.05 E-08	N.E.

N.E.=no efficacy

Figure legends

Figure 1 Construction and quality control of a synthetic nanobody library

A). Sequence alignment of a camel nanobody(1ZVH) with ASyNAL scaffold, showing the randomization regions in CDR H1, CDR H2&CDR H3 by X, respectively. The X is a mix of amino acids with the ratio showed below. B). NGS data(n.=20112) showing the amino acid occurrence rate of the ASyNAL at each position vs designed rate. 20112 nanobody sequences were aligned, the amino acid residues at CDR regions were retrieved and the rate of each amino acid occurrence at each position were calculated.

Figure 2 Identification of C5 clone as a spike protein/RBD binder and compete with both Spike and RBD binding to ACE2

Phage panning of the ASyNAL library against antigens RBD, S1 and spike protein respectively generated eight nanobody clones. Clone B7 is for RBD, A11 for S1 and C5, D3, D8, D9, F12, G6 are for spike protein. The cross reactivities of the eight clones to Spike(A), S1(B) and RBD(C) were determined by phage ELISA.Competitive ELISA showed that C5 phage and ACE2 competed each other to bind RBD(D) and the full length spike protein(E). As controls, B7 phage and D3 phage had no competition. F) Binding curve of C5 protein to RBD in BLI assay. The affinity is 18 nM.

Figure 3 Optimization of C5 clone by phage display led to the identification of C5G2 clone

A) C5 clone were used as template to generate a optimization library with mutation at all the CDRs. Panning of this library against RBD resulted in ten C5 variants. The CDR regions of these ten clones were aligned. The alignment represented by Weblogo were showed beneath each CDR region. B) C5G2 variant was purified from E. coli host and resolved in SDS-PAGE. C) Binding curve of C5G2 protein to RBD in BLI assay. The binding affinity increased from 18 nM to 1.62 nM. D) Size exclusion chromagraphy(SEC) profile of C5G2 protein resovled in a Tosho TSKgel G3000SW column.

Figure 4. Pseudovirus assay of C5G2 nanobody

A) Competitive ELISA showed C5G2 protein, but not D3, competed with ACE2 to bind RBD with a IC50 of 3.75 nM. As a control, the IC50 of mNb6 for competition was 4.64 nM. N=3. B) Pseudovirus assay of C5G2's inhibition potency to protect cells from virus infection. The wild type virus and Alpha, Beta Gamma, Delta and Omicron virus were test. mNb6 from (ref) was a positive control. Nanobody D3 binding to NTD of S1 was the negative control. The IC50 value were showed both in ng/ml and nM(nmol/L)

Figure 5. Structural basis for the broad neutralization of C5G2. (A-B) Cryo-EM density maps of SARS-CoV-2 spike protein in complex with C5G2 viewed from side (A) and top (B), respectively. C5G2 is colored in red and the up RBD, down RBD, NTD, glycans of spike are colored in teal, orange, blue and pink, respectively, the rest density of spike is colored in gray. **(C)** The 3.88 Å density map of local refinement of C5G2 and bound RBD and NTD. **(D)** Atomic model of G5G2:RBD:NTD. C5G2 is presented as cartoon and RBD and NTD are presented as surface representations, respectively. The epitopes of C5G2 on the RBD and NTD are both colored in teal. The decorated glycans on on RBD and NTD are shown as pink sticks. **(E-G)** the interaction details between C5G2 and RBD (E-F), NTD (G). C5G2 is showed as transparent cartoon and the RBD and NTD are shown as transparent surface. The residues involved in the hydrogen bond (gold dotted lines) interaction are shown as stick. The contacts between C5G2 and NTD are also presented as green dotted lines. **(H)** RBD sequences of SARS-CoV-2 WT and its 5 VOC variants (Alpha, Beta, Gamma, Delta and Omicron) with highlighted footprint of C5G2 (colored in light red).

Figures

Figure 1

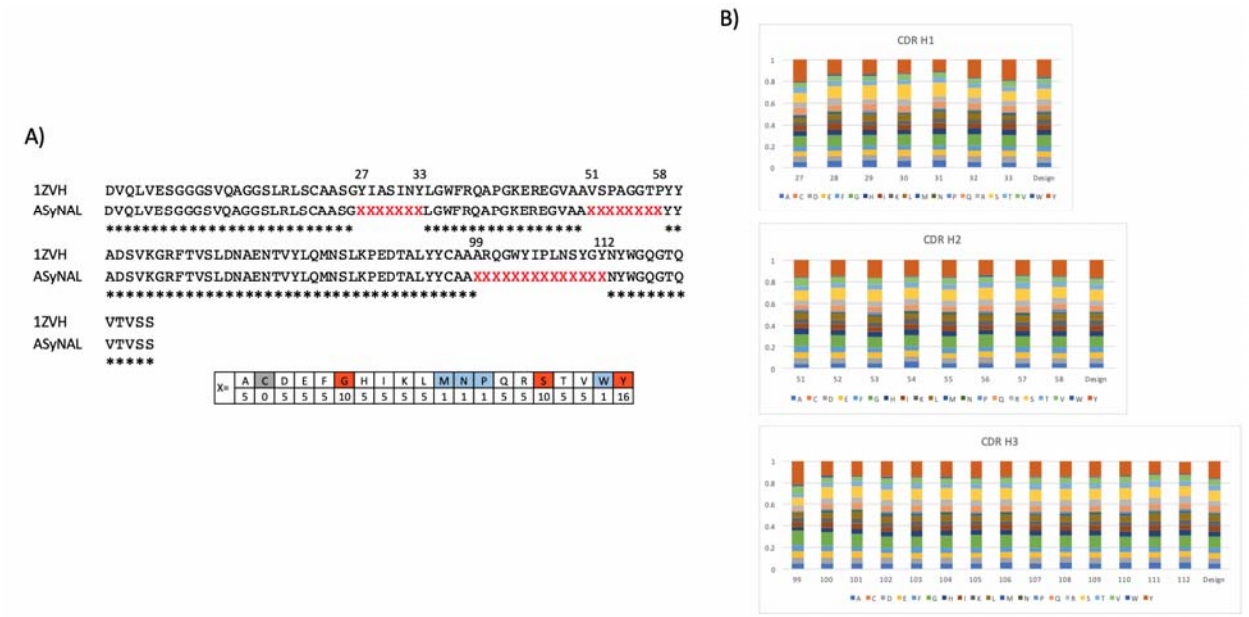

Figure 2

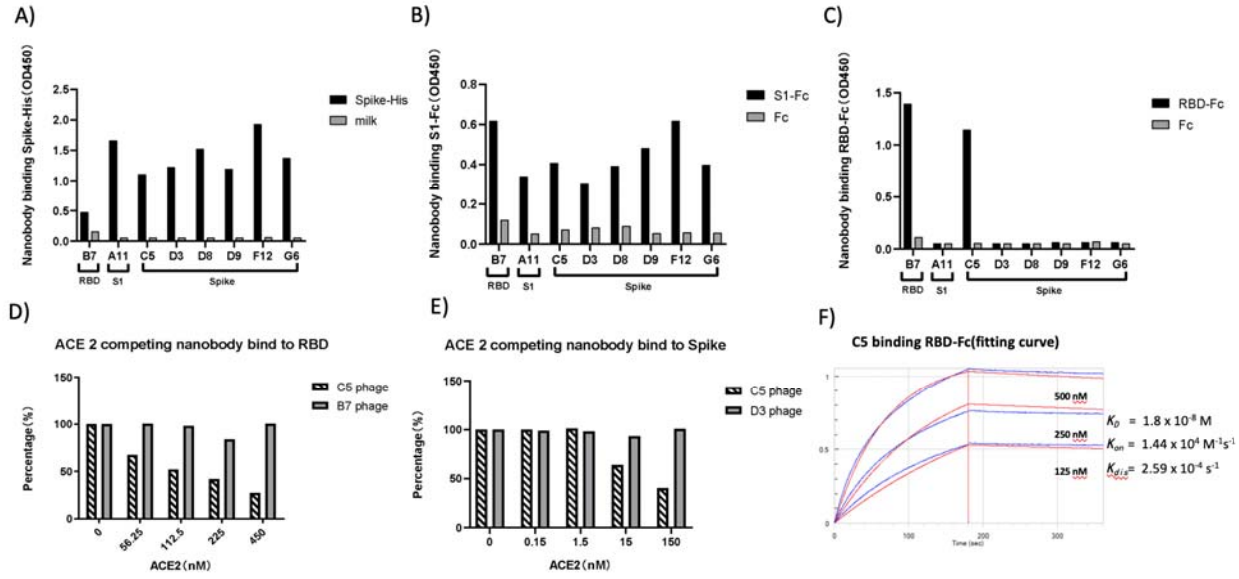

Figure 3

A)

	CDR H1							CDR H2								CDR H3													
position	27	28	29	30	31	32	33	51	52	53	54	55	56	57	58	99	100	101	102	103	104	105	106	107	108	109	110	111	112
C5 WT	K	Y	S	H	L	G	F	G	L	G	A	Y	E	D	G	L	V	V	F	S	R	D	S	P	E	F	L	A	Q
D2	E	Y	S	Q	L	R	F	G	L	G	A	N	E	D	G	L	V	I	F	S	H	D	G	P	E	F	L	A	Q
G2	K	F	S	H	L	V	F	G	L	G	A	Y	E	S	G	L	V	V	L	S	R	D	N	T	E	F	I	A	H
D3	E	W	S	H	L	R	F	G	L	G	S	Y	E	H	A	L	V	V	F	S	H	D	S	P	E	F	L	A	H
C2	E	Y	R	H	L	I	F	G	L	G	A	Y	V	D	R	L	V	V	F	S	E	D	S	R	E	F	L	A	H
B3	K	F	S	H	L	A	F	G	L	G	A	Y	E	D	V	L	V	V	F	S	H	D	R	A	E	F	L	A	H
B2	K	F	S	H	L	A	F	G	L	G	E	H	E	D	C	L	V	V	F	S	R	D	S	T	E	F	L	A	Q
H1	K	Y	S	H	L	A	F	G	L	G	A	Y	E	D	G	L	V	V	F	S	R	E	G	P	D	F	V	A	Q
E3	K	Y	S	H	L	S	F	G	L	G	A	N	E	D	A	L	V	V	F	S	N	D	S	S	E	F	L	A	Q
F3	K	Y	S	H	L	V	F	G	L	G	A	H	E	A	G	L	V	V	F	S	R	D	S	L	E	F	L	A	Q
F2	N	Y	S	F	L	R	F	G	V	G	A	N	E	N	S	L	V	V	F	S	G	D	S	P	E	F	L	A	H

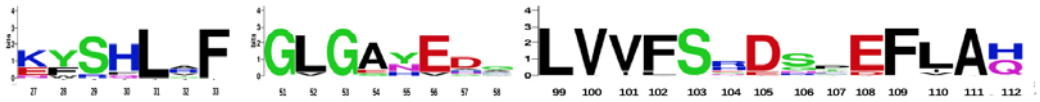

B)

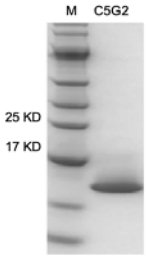

C)

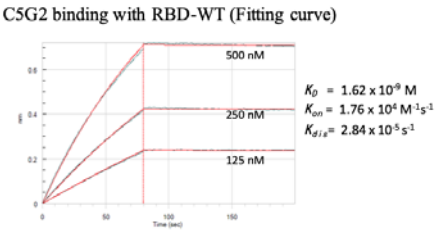

D)

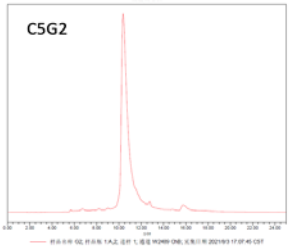

Figure 4

A)

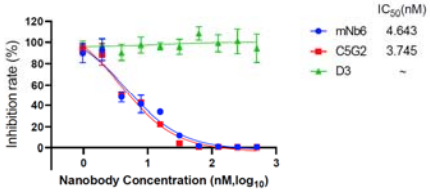

B)

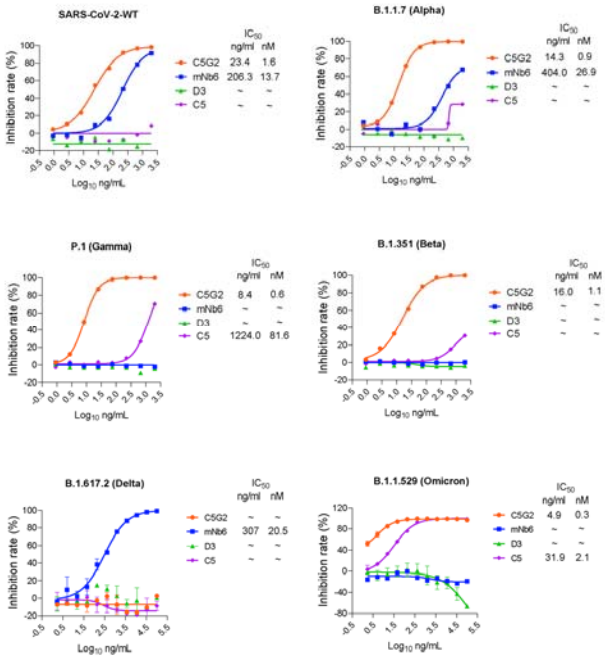

Figure 5

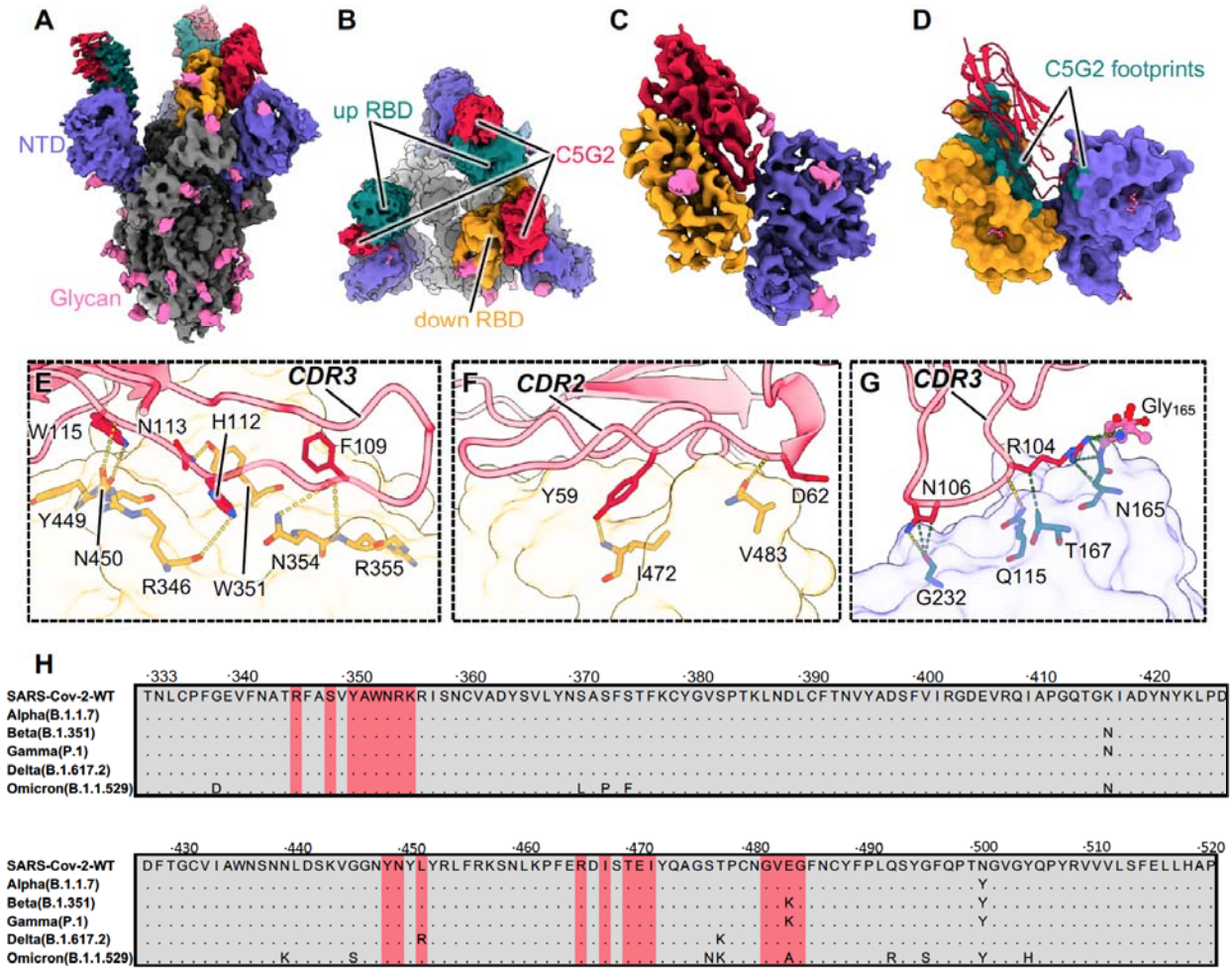
A
NTD
Glycan
B
up RBD
C5G2
down RBD
C
D
C5G2 footprints
E
CDR3
W115
N113
H112
F109
Y449
N450
R346
W351
N354
R355
F
CDR2
Y59
D62
I472
V483
G
CDR3
Gly165
R104
N106
N165
T167
Q115
G232
H
SARS-Cov-2-WT
Alpha(B.1.1.7)
Beta(B.1.351)
Gamma(P.1)
Delta(B.1.617.2)
Omicron(B.1.1.529)